




Structure of the NuA4 histone acetyltransferase complex

Liting Ji^{a,1}, Lixia Zhao^{a,1}, Ke Xu^{a,1}, Huihan Gao^a, Yang Zhou^a, Roger D. Kornberg^{a,b,2} , and Heqiao Zhang^{a,2}

Contributed by Roger Kornberg; received August 22, 2022; accepted October 24, 2022; reviewed by Cornelius Gati, Kenji Murakami, and Dong Wang

Nucleosome acetyltransferase of H4 (NuA4), one of two major histone acetyltransferase complexes in *Saccharomyces cerevisiae* specifically acetylates histone H2A and H4, resulting in increased transcriptional activity. Here we present a 3.8–4.0 Å resolution structure of the NuA4 complex from cryoelectron microscopy and associated biochemical studies. The determined structure comprises six subunits and appropriately 5,000 amino acids, with a backbone formed by subunits Eaf1 and Eaf2 spanning from an Actin-Arp4 module to a platform subunit Tra1. Seven subunits are missing from the cryo-EM map. The locations of missing components, Yaf9, and three subunits of the Piccolo module Esa1, Yng2, and Eaf6 were determined. Biochemical studies showed that the Piccolo module and the complete NuA4 exhibit comparable histone acetyltransferase activities, but the Piccolo module binds to nucleosomes, whereas the complete NuA4 does not. The interaction lifetime of NuA4 and nucleosome is evidently short, possibly because of subunits of the NuA4 complex that diminish the affinity of the Piccolo module for the nucleosome, enabling rapid movement from nucleosome to nucleosome.

NuA4 | histone acetyltransferase | cryo-EM

The nucleosome, the fundamental particle of the chromosome (1, 2), serves as a transcription barrier for almost all protein-coding genes (3). Posttranslational modifications (PTMs), which mainly occur on the histone tails, influence the chromatin context and therefore regulate transcription (4, 5). Histone acetylation is one of the well-studied PTMs that plays important roles in gene regulation and maintenance of genome integrity (6, 7). The level of histone acetylation is established through the combined actions of histone acetyltransferases (HATs) and histone deacetylases (HDACs) (8). The two major HATs in *S. cerevisiae* are the NuA4 (nucleosome acetyltransferase of H4) and SAGA (Spt-Ada-Gcn5-acetyltransferases) complexes (9). NuA4 preferentially acetylates histones H2A and H4 (10). In addition to histones, NuA4 also acetylates approximately 250 nonhistone substrates, thus serving to regulate a variety of cellular processes, including DNA repair, cell cycle progression, and chromosome stability (11–14).

NuA4, a 13-subunit complex with a molecular weight of 1.04 MDa, shares its largest subunit, Tra1, with SAGA, whose major substrate is histone H3 (15–17). NuA4 also shares four subunits, Eaf2, Arp4, Actin, and Yaf9, with the SWR1 chromatin remodeling complex; these four subunits correspond to DAMP1, BAF53a, Actin, and YEATS of the mammalian TIP60 complex (13, 18). The Piccolo module of NuA4, comprising Epl1, Eaf6, Yng2, and the catalytic subunit Esa1, is responsible for HAT activity (19). The TINNTIN module, consisting of Eaf3, Eaf5, and Eaf7, interacts with phosphorylated RNA polymerase II and so is involved in the transcription elongation process (20). Biochemical studies have identified Eaf1 as an assembly platform for the other subunits of NuA4 (21). Structural information on NuA4 is limited to an X-ray crystal structure of a truncated form of the Piccolo module at 2.8 Å (22) and a cryo-EM reconstruction of a complex of Tra1, Eaf1, Eaf5, Actin, and Arp4 (so-called TEEAA module) at 4.7 Å (23). Despite many years' studies, the high-resolution structural information of NuA4 still remained missing; here, we present the structure of the NuA4 complex at an overall resolution of 3.8–4.0 Å through cryoelectron microscopy.

Results

Purification and Structure Determination of the Complete NuA4 Complex. We fused a TAP tag to the C terminus of the Epl1 subunit of the Piccolo module and purified the complete NuA4 complex to homogeneity by tandem-affinity purification and glycerol gradient centrifugation (Fig. 1A and *SI Appendix*, Fig. S1A). Mass spectrometry confirmed the presence of all subunits of the NuA4 complex (*SI Appendix*, Table S1). SDS-PAGE showed that the subunits were approximately equimolar (Fig. 1A). The catalytic activity of the purified NuA4 complex was confirmed by the reaction of nucleosomes formed on either 217 bp or 147 bp DNA with acetyl coenzyme A. The 217 bp nucleosomes (217-

Significance

The structure of NuA4, one of two major histone acetyltransferases of *Saccharomyces cerevisiae*, is reported at 3.8 Å resolution. Six polypeptide chains of the complex, comprising about half the total mass, could be traced. This region is conserved from yeast to humans. Part of the complex performs a negative role, diminishing the affinity of the acetyltransferase for the nucleosome.

Author affiliations: ^aShanghai Institute for Advanced Immunochemical Studies, ShanghaiTech University, Shanghai 201210, China; and ^bDepartment of Structural Biology, Stanford University School of Medicine, Stanford, CA 94305

Author contributions: H.Z. designed research; L.J., L.Z., K.X., H.G., and Y.Z. performed research; H.Z. analyzed data; and R.D.K. and H.Z. wrote the paper.

Reviewers: C.G., University of Southern California; K.M., University of Pennsylvania; and D.W., University of California San Diego.

The authors declare no competing interest.

Copyright © 2022 the Author(s). Published by PNAS. This open access article is distributed under [Creative Commons Attribution-NonCommercial-NoDerivatives License 4.0 \(CC BY-NC-ND\)](https://creativecommons.org/licenses/by-nc-nd/4.0/).

¹L.J., L.Z., and K.X. contributed equally to this work.

²To whom correspondence may be addressed. Email: kornberg@stanford.edu or zhanghq@shanghaitech.edu.cn.

This article contains supporting information online at <https://www.pnas.org/lookup/suppl/doi:10.1073/pnas.2214313119/-/DCSupplemental>.

Published November 22, 2022.

NCP) proved to be a better substrate for acetylation than the 147 bp nucleosomes (147-NCP) (Fig. 1A).

Cryoelectron microscopy was used to determine the structure of the NuA4 complex. After grid preparation, we noticed that the NuA4 complex tends to fall apart. To get a homogenous and stable sample for structure determination, glycerol gradient centrifugation and crosslinking were performed. Peak glycerol gradient fractions and crosslinking were performed. Peak glycerol gradient fractions were pooled, concentrated, and cross-linked, followed by cryo-EM analysis (SI Appendix, Fig. S1 B and C). After multiple rounds of data processing (SI Appendix, Fig. S2A), a NuA4 map was obtained at 4 Å resolution (Fig. 1B). Local refinement was performed for the core module (which lacks the “Lasso” region of Tra1, Fig. 1B) in cryoSPARC, yielding a 3.8 Å map (Fig. 1B and SI Appendix, Fig. S2 B and C). An atomic model, built by homology modeling, assisted by AlphaFold prediction (SI Appendix, Table S2), fits well to the maps (Fig. 1 C and D and SI Appendix, Fig. S3).

Overall Structure of NuA4. Six subunits, Eaf1, Eaf2/Swc4, Actin, Arp4, Epl1, and Tra1, are present in the map (Fig. 2A), while three subunits of the Piccolo module, Esa1, Yng2, and Eaf6, and the entire TINNTIN module are absent (Fig. 1C), likely due to motion or disorder. There are differences from the previously published 4.7 Å resolution map, in which Eaf2/Swc4 and Eaf5 were apparently incorrectly assigned (23). The Actin-Arp4 module is connected to Tra1 through a “Neck” region, consisting of the C-terminal domain of Epl1, the post-SANT domain of Eaf2, and flanking sequences of the HSA domain of Eaf1 (Fig. 2 A and B). The SANT domain of Eaf2, with a conserved helical feature (whose density was misassigned to Eaf1 in the previous study), stacks against the side of Arp4 (Fig. 2A).

Eaf1 and Eaf2 Act as the Backbone of the NuA4 Complex. The structure confirms the inference from a previous biochemical study

that Eaf1 serves as a backbone of the NuA4 complex (21) and demonstrates a similar role for Eaf2/Swc4. Both Eaf1 and Eaf2/Swc4 exhibit extended conformations, twisting about each other, spanning from the Actin-Arp4 module to the FAT domain of Tra1 (Fig. 2 A and B). The structure indicates that all sequence features of Eaf1 (Eaf1-NTD, pre-HSA, HSA, and C-terminal MyB-like domain), and all sequence features of Eaf2 (Eaf2-NTD, SANT, and post-SANT domains), are likely essential for their backbone roles (Fig. 2B).

The Actin-Arp4 Module is Stabilized by Both the Eaf1-HSA and by the Eaf2-NTD. The Actin-Arp4 module is conserved and shared by NuA4, SWR1, INO80, and mammalian PBAF complexes (23–26). The Eaf1-HSA domain, also conserved among all complexes (Fig. 3E), resembles a latch, stabilizing the Actin-Arp4 module (Fig. 3A). Glu365, Asp373, and several hydrophobic residues of Eaf1-HSA contribute to the interaction with the Actin-Arp4 module. The N-terminal β-sheet of Eaf2 also binds the Actin-Arp4 module (only in NuA4, apparently not in the SWR1, INO80, and PBAF complexes) with several hydrogen bonds formed by Trp94, Trp78, Asn86, Ser88, Thr90, and Tyr111 from Eaf2, Glu117, Glu125, and Tyr362 from Actin and Glu135, Trp469, and Glu474 from Arp4 (Fig. 3B). Asp373 of the HSA domain also hydrogen bonds with Arg644 of Epl1 (Fig. 3 C and D). Extra density in the nucleotide-binding pocket of Arp4 was observed and eventually assigned to ATP (Fig. 3F). The binding pocket and the ATP-interacting residues (Fig. 3F) resemble those in the structure of Actin-Arp4 module complexed with the SWR1 HSA (24). In both NuA4 and SWR1 structures, an ATP molecule is associated with Arp4 but not with Actin. We asked whether ATP binding and hydrolysis might influence the HAT activity of NuA4 and found no effect of ATP, ADP, or the ATP-analog AMP-PNP (Fig. 3G).

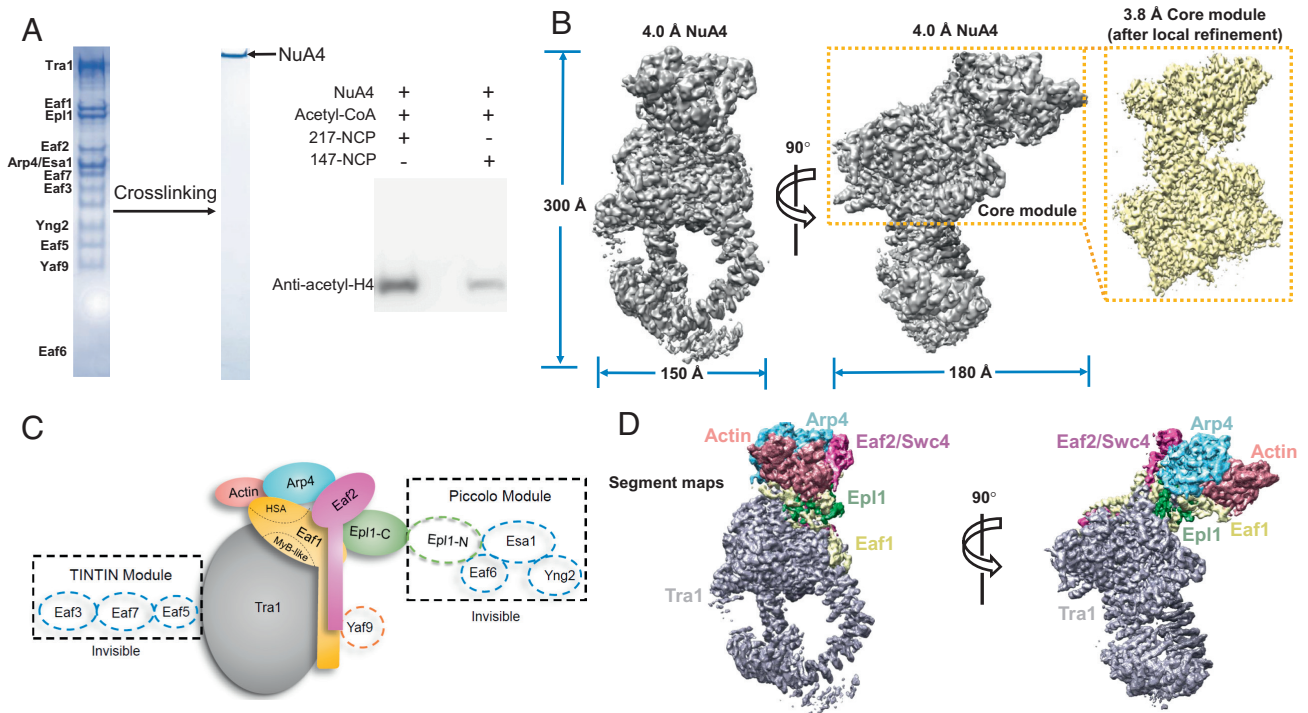


Fig. 1. Biochemical and cryo-EM studies of *S. cerevisiae* NuA4 complex. (A) From Left to Right are the SDS-PAGE bands, crosslinked band of NuA4, and histone acetyltransferase (HAT) assay of NuA4 against different NCP substrates. (B) Electron density map of the NuA4 complex, rotated by 90°. The right panel is an expanded view of a 3.8 Å electron density map of the core module after local refinement. (C) A scheme of the NuA4 complex. Invisible subunits are indicated with dashed boxes. (D) Segmentation of the electron density map, rotated by 90°. Each subunit is indicated and labeled.

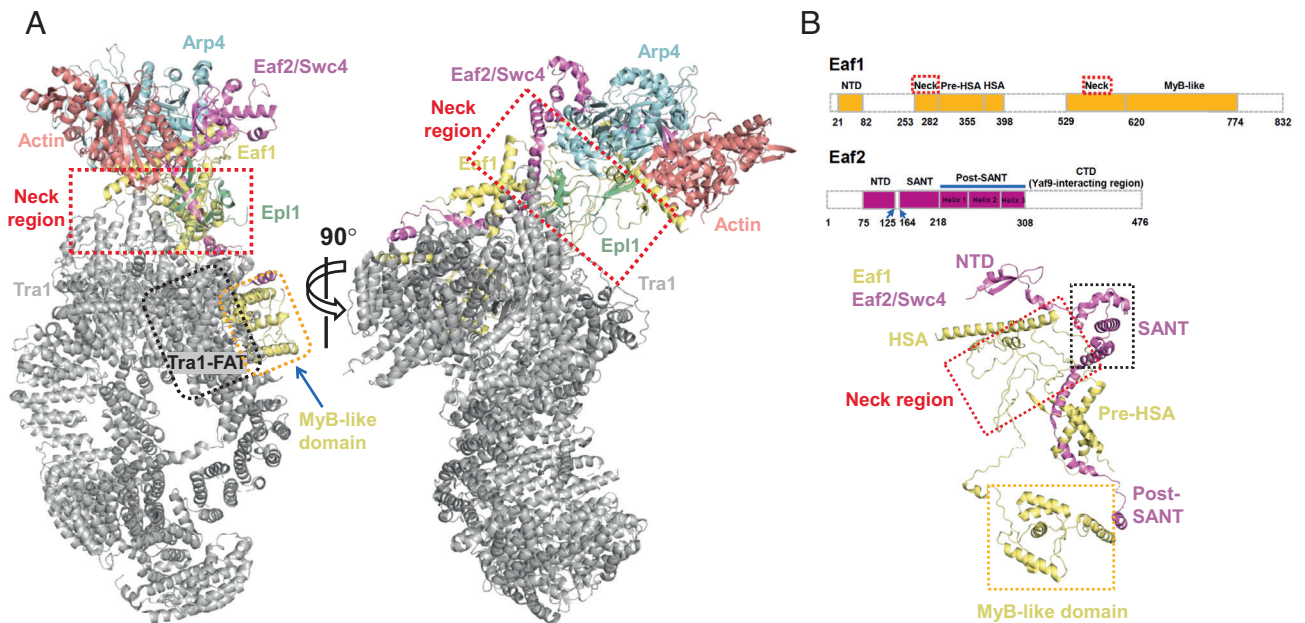


Fig. 2. Overall structure of the NuA4 complex. (A) Ribbon diagrams of NuA4 subunits, rotated by 90°. Each subunit is indicated with different colors. The “Neck” region, the FAT domain of Tra1, and the MyB-like domain of Eaf1 are indicated with dashed squares, respectively. (B) From *Top to Bottom* are the domain organizations of Eaf1 and Eaf2 and the structure of Eaf1-Eaf2. Residues at domain boundaries are indicated at the *Bottom*.

Structure of the Neck Region and Implications for the Location of the Piccolo Module. Improving the resolution of the Neck region to 3.0–3.2 Å revealed that this region, previously attributed to Eaf1 alone (23), is composed of the HSA-flanking sequences of Eaf1,

the post-SANT domain of Eaf2, and the C-terminal domain of Epl1 (Figs. 2 *A* and 4*A*). The β-strands of Eaf1 and C-terminal β-strands of Epl1 form two hybrid β-sheets, in one of which an Eaf1 strand is sandwiched between two of Epl1, a different

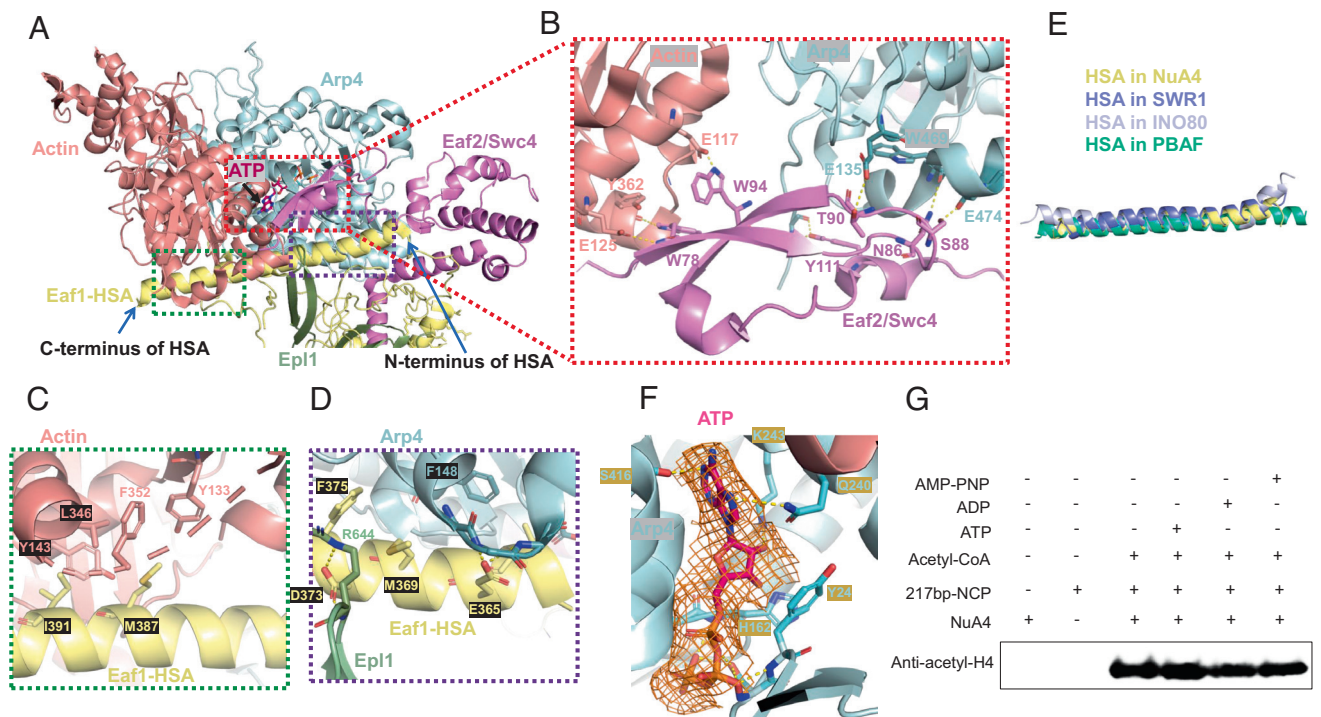


Fig. 3. Structures of Actin-Arp4 module in complex with HSA and Eaf2-NTD. (A) Ribbon diagrams of Actin-Arp4-HSA-Eaf2-Epl1. Each subunit is indicated with different colors. An ATP molecule is shown as sticks and labeled. The HSA domain of Eaf1 and its N and C termini are labeled. (B) Structure of Actin-Arp4-Eaf2. The interacting residues are shown as sticks and labeled in different colors (same as the colors of corresponding subunits they belong to). (C) and (D) are the C-terminal and N-terminal interfaces between Eaf1-HSA and the Actin-Arp4 module. The interacting residues are shown as sticks and labeled in different colors (same as the colors of corresponding subunits they belong to). (E) Structure comparison of the HSA domains in NuA4, SWR1, INO80, and PBAF complexes. (F) An ATP molecule and the corresponding electron density are shown as sticks and meshes, respectively. The ATP-interacting residues of Arp4 are shown as sticks and labeled. (G) HAT assay of NuA4 against 217-NCP performed in the presence of acetyl-CoA and in the absence or presence of ATP, ADP, and AMP-PNP. Different reaction times are labeled at the bottom of the bands.

mode of subunit–subunit interaction, insofar as we can determine (Fig. 4B). The N-terminal residue of Epl1 in the map is Thr539, and the sequence preceding this residue interacts with the Piccolo subunit Esa1 (22), thereby identifying the potential location of the Piccolo module (Fig. 4B).

Potential Location of Yaf9. Three α -helices of the post-SANT domain of the Eaf2 subunit are denoted tethering helices 1, 2, and 3 in view of their role in connecting the Arp4 protein to the FAT domain of Tra1 (Fig. 5). The C terminus of Eaf2 is required for interaction with Yaf9 (21), a histone-tail binding subunit of NuA4, and the binary structure of Eaf2–Yaf9 could be predicted by an AlphaFold-Multimer (Fig. 5B) (27). Despite slight bending of tethering helices 1 and 2 in our structure, compared with a single long tethering helix in the predicted structure, the overall conformation and the location of tethering helix 3 in our structure are similar to those in the predicted one (Fig. 5A and B). In the predicted structure, the C-terminal domain of Eaf2 (residues 324 to 476) forms a complex with Yaf9 (Fig. 5B). Taking into account the length of the linker between tethering helix 3 and the C-terminal domain, we could predict that the potential location of Yaf9 is adjacent to the FAT domain of Tra1 rather than the Actin–Arp4 module as previously proposed.

Influence of NuA4 Subunits upon Piccolo–Nucleosome Interaction. NuA4 purified from yeast, and the Piccolo module expressed in insect cells, exhibited comparable histone acetylation activities (Fig. 6A), but they appear to differ in affinity for nucleosomes. When NuA4 and nucleosomes were mixed and subjected to glycerol gradient sedimentation, they separated, failing to form a stable complex (Fig. 6B), consistent with a previous study showing that NuA4 alone does not associate with the nucleosome (28). By contrast, the Piccolo module formed a complex with a nucleosome in an electrophoretic mobility shift assay, consistent with previous studies (Fig. 6C) (22, 29). These data suggest that components of NuA4 diminish the affinity of the Piccolo module for nucleosomes, limiting the lifetime of the interaction.

Discussion

It is worth noting that seven components of the NuA4 complex are missing from our cryo-EM map, likely due to motion. We cannot rule out another possibility that these subunits dissociated during cryo-EM grid preparation.

NuA4 and SAGA, the two major histone acetyltransferase complexes in *S. cerevisiae*, have the same largest subunit, Tra1, but differ in all other components. The difference in subunit composition is not due to a difference in Tra1 conformation between the two complexes, because the two structures are closely similar, with an RMSD (root mean square deviation) of 1.002 Å over 3,404 C α atoms. The NuA4-specific subunits are associated with a different surface of Tra1 from the SAGA-specific subunits (SI Appendix, Fig. S4), so it may be asked why all these subunits do not interact simultaneously. The answer is that the C-terminal MyB-like domain of Eaf1 binds to the surface occupied by SAGA-specific subunits (SI Appendix, Fig. S4), ensuring the formation of two distinct complexes.

The NuA4-specific and SAGA-specific subunits impart distinct properties, such as affinity for the nucleosome. NuA4–nucleosome interaction is likely transient, whereas SAGA forms a stable complex, as shown elsewhere by electrophoretic mobility shift assay. SAGA-specific subunits may contribute to nucleosome interaction, whereas NuA4 subunits interfere with the interaction. Structures of NuA4–nucleosome and SAGA–nucleosome complexes are needed to elucidate the matter. Whether the transcriptional activators would enhance the NuA4’s nucleosome binding affinity remains to be investigated.

Materials and Methods

Purification of Yeast NuA4 Complex and its Piccolo Module. First, 40 liters of *S. cerevisiae* cells with Epl1 bearing a C-terminal TAP tag were grown at 30°C and harvested at OD₆₀₀ \approx 10 by centrifugation. Cell pellets were resuspended in lysis buffer A (100 mM HEPES, pH 8.0, 600 mM NaCl, 6 mM DTT, and 2 \times EDTA-free protease inhibitor cocktail) and then homogenized to prepare the whole-cell extraction. To get rid of contaminated nucleic acid, 0.25% (v/v) PEI precipitation was applied. The supernatant containing the protein of interest was

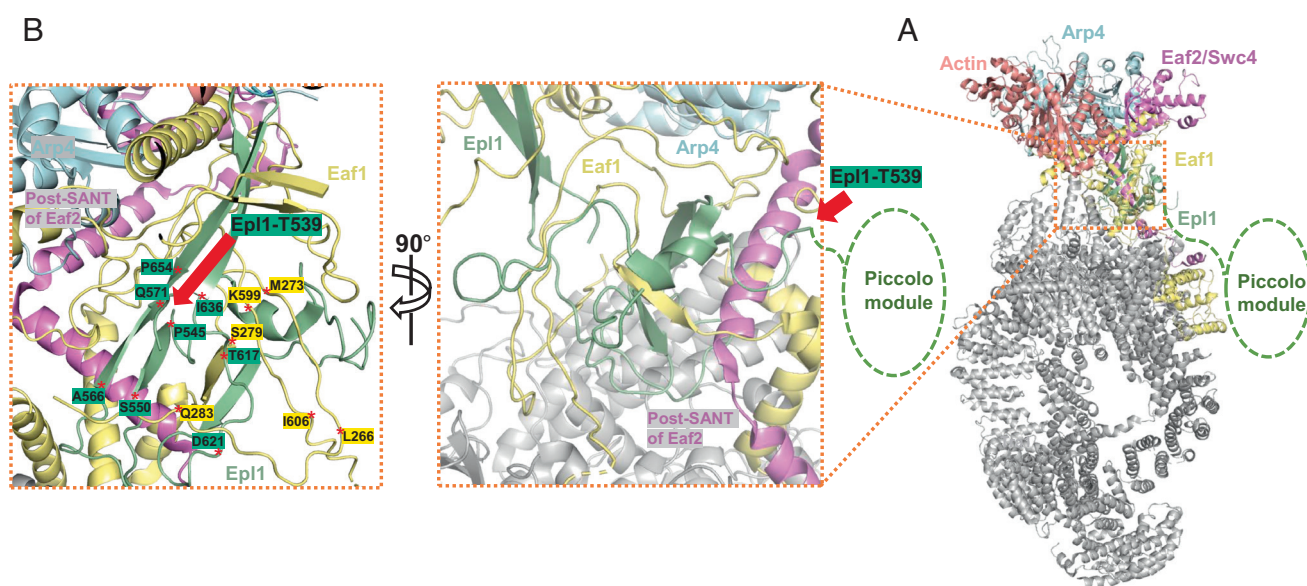


Fig. 4. Structures of the “Neck” region. (A) Ribbon diagrams of NuA4. The Neck region is indicated with a salmon dashed square. (B) Expanded view of the Neck region formed by Eaf1, Eaf2, and Epl1, rotated by 90°. Residues at the β -strand boundaries are indicated and labeled with different backgrounds. The amino acid T539 of Epl1 is indicated with a red arrow, and the possible position of Piccolo module is indicated with a green circle.

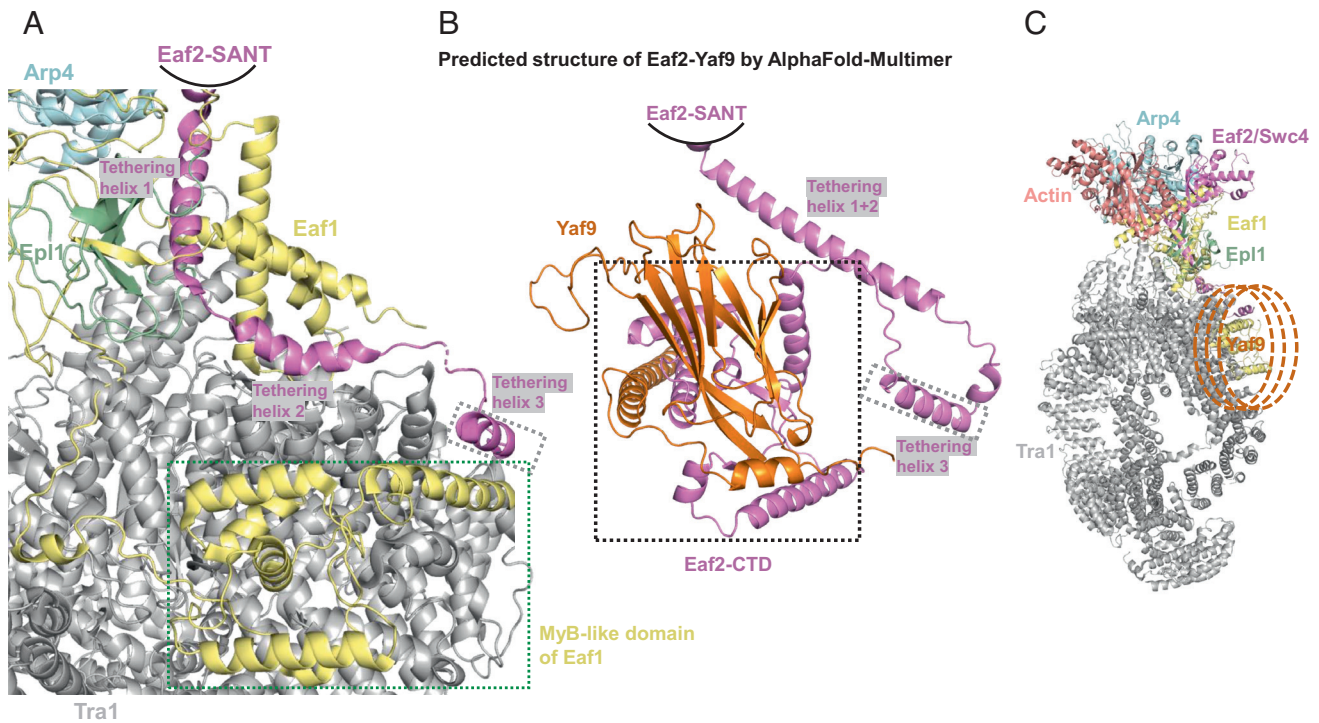


Fig. 5. A possible binding position of Yaf9. (A) Ribbon diagrams of the interaction among the post-SANT domain of Eaf2, Eaf1, and Tra1. Each subunit is indicated with different colors, and the tethering helices are labeled. (B) The predicted structure of Eaf2-Yaf9 by an AlphaFold-Multimer. The tethering helices are labeled and the C-terminal domain of Eaf2 is indicated with a black dashed square. (C) The position of Yaf9 in NuA4. The possible positions of Yaf9 are indicated with orange dashed circles.

further precipitated using 50% (v/v) ammonium sulfate, and the precipitation was dissolved with buffer B (50 mM HEPES, pH 8.0, 25 mM ammonium sulfate, 3 mM DTT, and 1X EDTA-free protease inhibitor cocktail). The solute was further cleared by centrifugation (8,000 rpm, 4°C, 90 min) and the supernatant was then pumped through IgG Sepharose-6 Fast Flow resin (GE Healthcare) at 4°C overnight. After extensively washing with buffer containing 50 mM HEPES, pH 8.0, 150 mM ammonium sulfate, and 3 mM DTT, overnight on-column cleavage was performed by adding TEV protease into the IgG resin. The eluate was then concentrated and subjected to 10 to 30% glycerol gradient centrifugation (40,000 rpm, 4°C, 10 h). The peak fractions were pooled, dialyzed against buffer C (25 mM HEPES, pH 8.0, 200 mM NaCl, and 3 mM DTT) and concentrated to approximately 1 mg/ml before grid preparation. To protect the NuA4 complex from falling apart, the concentrated sample was crosslinked by 0.1% (v/v) glutaraldehyde in the presence of 0.01% NP40 (v/v) on ice for 10 min before grid freezing.

We had previously attempted to overexpress the full-length Piccolo module through the bacteria system but failed to obtain a stoichiometric complex. We therefore chose the baculovirus expression system. The genes encoding all the subunits of the Piccolo module, including Esa1, Epl1, Eaf6, and Yng2, were amplified from the genomic DNA of *S. cerevisiae* and cloned into pFastBac-1 vector with a 6× His tag at the N terminus of Epl1 and a Flag tag at the C terminus of Esa1. Each baculovirus was produced using the Bac-to-Bac baculovirus expression system (Invitrogen). The Piccolo module was overexpressed in High Five cells by coinfection of four baculovirus for 48 h at 27°C. One liter of High Five cells (2.0×10^6 cells ml⁻¹ cultured in ESF921 medium) was harvested and centrifuged. The cell pellets were resuspended with buffer containing 25 mM HEPES, pH 8.0, 300 mM NaCl, and 3 mM DTT and lysed by sonication. The lysate was cleared by centrifugation, purified using Ni-NTA (Qiagen) and anti-Flag columns (Genscript), and further cleaned using Heparin and size-exclusion chromatography (Superdex 200, GE Healthcare) in buffer containing 25 mM HEPES, pH 8.0, 100 mM NaCl, and 3 mM DTT. The peak fractions were concentrated to ~1 mg/ml before use.

Vitrobot Mark IV was used for grid plunging. Before grid freezing, 300-mesh Quantifoil R1.2/1.3 grids were glow-discharged. Then, 3 μl of crosslinked NuA4 complex was applied to the grid. After incubation for 60 s, the grid was blotted for 2.5 s before being plunged into liquid ethane with 100% chamber humidity at 8°C. All grids were stored in liquid nitrogen until data collection.

The *Xenopus* histone octamer was overexpressed, purified, and reconstituted with 147 bp and 217 bp Widom-601 DNAs as described previously (30). The 217 bp (ATCTGAGAATCCGGTGCCGAGGCCGCTCAATTGGTCGTAGACAGCTCTAGCACCGCTAAACGCACGTACGCGCTGTCCCGCGTTTTAACCGCCAAGGGATTACTCCC TAGTCTCCAGGCACGTGTCAGATATATACATCCGATATCGGATCCTCT-AGAGTCGACCTG CAGGATCGAAGCTTGGCGTAATCATGGTCATAGCTGTTTCTGTG) and 147 bp DNA (ATCGAGAATCCCGGTGCGGAGGCCGCTC-AATTGGTCGTAGACAGCTCTAGCACCGC TTAACGCACGTACGCGCTGTCCCGCGTTTTAACCGCCAAGGGATTACTCCC TAGTCTCCAGGCACGTGTCAGATATATACATCCTGAT) were used to reconstitute nucleosomes as described previously (30).

Cryo-EM Data Collection and Image Processing. Automated data acquisitions were performed using SerialEM (31) on a Titan Krios equipped with a Gatan K3 Summit direct electron detector (Gatan, Inc.) and operating at 300 kV with a nominal magnification of 18,000× and a pixel size of 0.66 Å (super-resolution mode). A total of 13,769 images were automatically recorded in the super-resolution mode, with a defocus range from 1.3 to 2.0 μm. Each movie stack was dose-fractionated to 40 frames with a total electron dose of ~60 e⁻/Å² and a total exposure time of ~3.4 s. Movie stacks were motion-corrected and the defocus value was estimated using the modules in cryoSPARC (32). The particles were first automatically picked using Blob Picker. The picked particles were extracted with a box size of 800 pixels (bin = 2), followed by 3 rounds of 2D classification, generating a template for subsequent template-based picking. A total of 2,742,073 particles picked from Template Picker in CryoSPARC were extracted with a box size of 800 pixels (bin = 2) and then subjected to 5 rounds of 2D classification. The particles assigned to the best class were reextracted with a box size of 520 pixels (bin = 1) and subjected to ab initio reconstructions (number of classes = 6), followed by 2 rounds of heterogeneous refinement. Nonuniform (NU) refinement was performed for the best class selected from the last round of heterogeneous refinement, yielding a reconstruction of NuA4 at 4 Å. To improve the resolution of the core module, a mask for the core module and another mask for the remaining parts of NuA4 were generated using Chimera, and the latter mask was used for particle subtraction in cryoSPARC (32). A further round of heterogeneous refinement and local refinement were applied for the best class of the core module using the former mask, resulting to a 3.8 Å reconstruction of the core module.

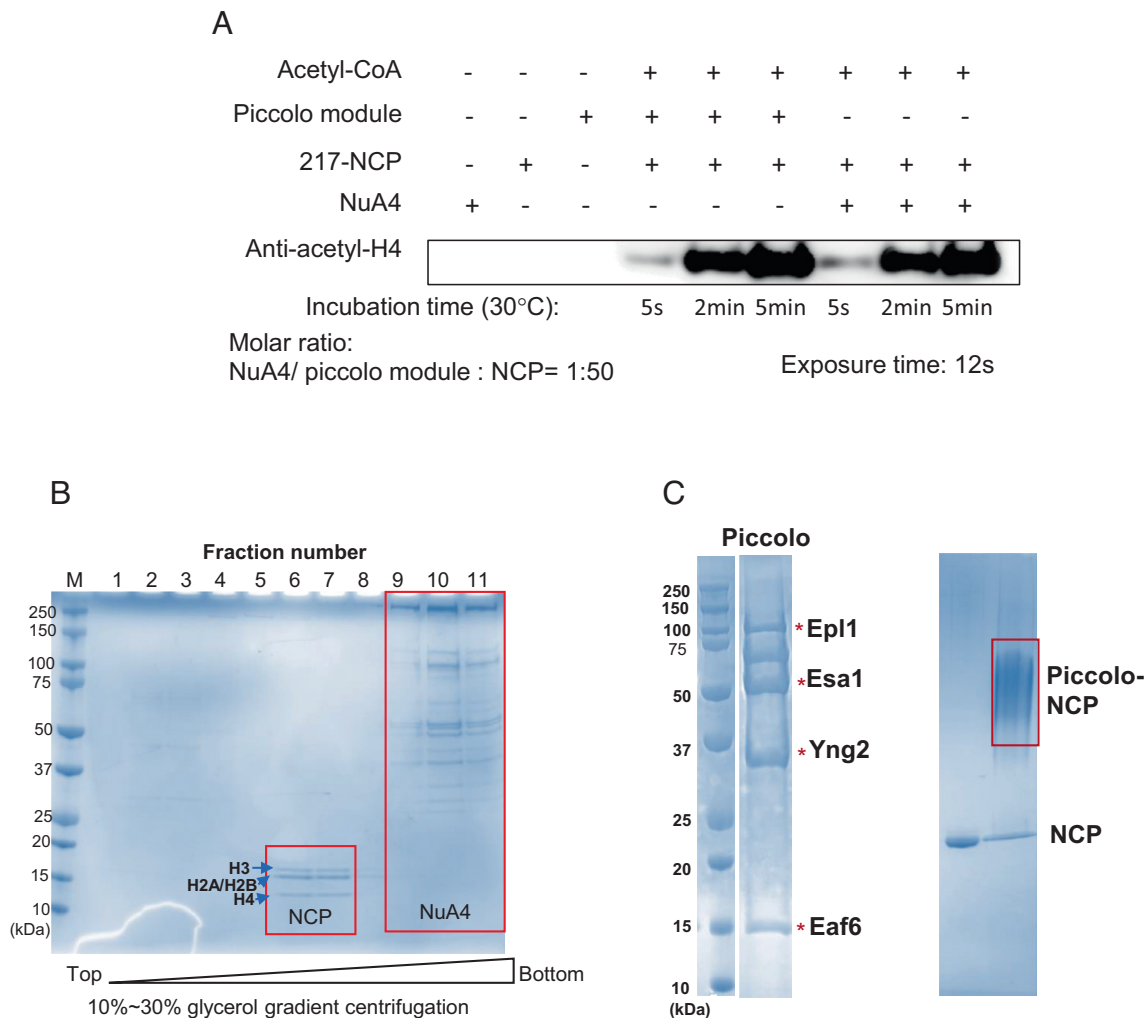


Fig. 6. The differences of NuA4 and its Piccolo module on nucleosome binding and acetylation. (A) Comparison of the HAT activity of NuA4 and its Piccolo module. The HAT reactions were quenched at time points of 5 s, 2 min, and 5 min, respectively. The exposure time for NuA4 and Piccolo module is 12 s. (B) Glycerol gradient sedimentation of 217-NCP-NuA4. Gradients were fractionated in 500 μ l, loaded on a 12% SDS-PAGE gel, and visualized by Coomassie blue staining. The peak fractions of NuA4 and NCP migrated at different positions are indicated with red squares. The histone proteins are indicated with blue arrows and labeled. (C) From top to bottom are the SDS-PAGE analysis of purified Piccolo module and the gel-shift result of the Piccolo module against the nucleosome, visualized by Coomassie blue staining.

Model Building. All the model buildings were performed using the cryo-EM module of Phenix package (33), Chimera (34), and COOT (35).

The 3.7 Å atomic model of Tra1 (PDB entry: 5OJS) (36) was docked into our 3.8 Å Cryo-EM map using Chimera (34) and then manually adjusted in COOT (35).

The long and flexible linkers in AlphaFold-predicted structures of Actin and Arp4 were first deleted using COOT (35) and then docked into the 3.8 Å Cryo-EM map of the core module using Chimera (34).

The remaining parts of the cryo-EM maps were successfully assigned to three subunits including Epl1, Eaf1, and Eaf2, owing to the relatively higher resolution of these regions and the consistencies between the map features and the AlphaFold-predicted structures.

All above-mentioned separate models were merged, and then subjected to Phenix for several rounds of real-space refinement. All the structure figures were generated by PyMOL (<https://pymol.org/2/>) and Chimera (34).

Histone Acetyltransferase Assay. All the reactions mentioned in the manuscript were performed in reaction buffer containing 25 mM HEPES (pH 8.0), 50 mM ammonium sulfate, 3 mM DTT, 100 μ M acetyl-CoA, and 1 μ M NCP (217-NCP or 147-NCP). To test the effects of different nucleotides on the reaction, 0.1 μ M NuA4 and equal molar of the corresponding nucleotides were added to the reaction buffer and incubated at 30°C, respectively. To compare the catalytic activity of NuA4 and the Piccolo module, 20 nM NuA4 and an equal molar of Piccolo proteins were added to the reaction buffer, respectively, and then were

allowed to react for 5 s, 2 min, and 5 min at 30°C, respectively. All the reactions were quenched by adding 5 \times SDS loading buffer and heated to 100°C for 5 min. The reaction mixtures were loaded to a 12% SDS-PAGE gel and subsequently analyzed using the primary antibody against acetylated-lysine of H4 (Abcam). The signals were quantified by ChemiDoc (Bio-Rad).

Gel-Shift Assay. To test the interaction, Piccolo module of NuA4 was mixed with an equal molar of NCP for an hour on ice, and then were loaded on a 3–12% Native-PAGE gel and detected by Coomassie blue.

Glycerol Gradient Centrifugation. Purified NuA4 and an equal molar of 217-NCP were incubated for 1 h on ice in the buffer containing 25 mM HEPES (pH 8.0), 50 mM ammonium sulfate, 3 mM DTT, and 5 mM MgCl₂. The mixture was applied to a 10–30% glycerol gradient in the same buffer and ultracentrifuged at 40,000 rpm (SW41 rotor) for 7 hours at 4°C. The gradients were fractionated in 500 μ l and analyzed with SDS-PAGE. The gels were stained with Coomassie blue.

Mass-Spectrometry. The NuA4 sample was excised from SDS-PAGE gel and was then reduced, alkylated, and treated by trypsin (Promega). After desalting and vacuum drying, the obtained peptides were dissolved in 0.1% FA and then were separated and analyzed by label-free quantification on an Easy-nLC 1000 system coupled to a Q Exactive HF (Thermo Scientific). Raw data were processed using MaxQuant (v.1.6.5.0) according to the *S. cerevisiae* Uniprot FASTA database. Two missed cleavage sites of trypsin were allowed, and the other parameters were

set as below: mass error of precursor ions: 5 ppm; fragment ions: 0.02 Da; the selected fixed-modifications: carbamidomethylation, oxidation (M), deamidation (NQ), and acetylation (protein N-term); false discovery rate thresholds: 1%, and minimum peptide length allowed: 7.

Data, Materials, and Software Availability. Cryo-EM maps for the core module of NuA4 and entire NuA4 complexes have been deposited in the Electron Microscopy Data Bank (EMDB) under accession codes [EMD-33794](#) and

[EMD-33796](#). Coordinates for the models have been deposited in the Protein Data Bank (PDB) under accession numbers [7YFN](#) and [7YFP](#), respectively. All study data are included in the article and/or [SI Appendix](#).

ACKNOWLEDGMENTS. We are grateful to Ms. Chengqian Zhang for mass spectrometric analysis. We thank the Bio-Electron Microscopy Facility of ShanghaiTech University for assistance in data collection. The research was supported by a grant from ShanghaiTech University.

1. J. Widom, Structure, dynamics, and function of chromatin in vitro. *Annu. Rev. Biophys. Biomol. Struct.* **27**, 285–327 (1998).
2. R. D. Kornberg, Chromatin structure: A repeating unit of histones and DNA. *Science* **184**, 868–871 (1974).
3. Y. Lorch, J. W. LaPointe, R. D. Kornberg, Nucleosomes inhibit the initiation of transcription but allow chain elongation with the displacement of histones. *Cell* **49**, 203–210 (1987).
4. B. A. Benayoun, R. A. Veitia, A post-translational modification code for transcription factors: Sorting through a sea of signals. *Trends Cell Biol.* **19**, 189–197 (2009).
5. S. Zhao, C. D. Allis, G. G. Wang, The language of chromatin modification in human cancers. *Nat. Rev. Cancer* **21**, 413–430 (2021).
6. M. Grunstein, Histone acetylation in chromatin structure and transcription. *Nature* **389**, 349–352 (1997).
7. T. Jenuwein, C. D. Allis, Translating the histone code. *Science* **293**, 1074–1080 (2001).
8. L. Icardi, K. De Bosscher, J. Tavernier, The HAT/HDAC interplay: Multilevel control of STAT signaling. *Cytokine. Growth Factor Rev.* **23**, 283–291 (2012).
9. D. Helmlinger, L. Tora, Sharing the SAGA. *Trends Biochem. Sci.* **42**, 850–861 (2017).
10. M. C. Keogh *et al.*, The *Saccharomyces cerevisiae* histone H2A variant Htz1 is acetylated by NuA4. *Genes. Dev.* **20**, 660–665 (2006).
11. R. Marmorstein, Structure and function of histone acetyltransferases. *Cell Mol. Life Sci.* **58**, 693–703 (2001).
12. M. J. Carrozza, R. T. Utley, J. L. Workman, J. Cote, The diverse functions of histone acetyltransferase complexes. *Trends Genet.* **19**, 321–329 (2003).
13. M. Squatrito, C. Gorrini, B. Amati, Tip60 in DNA damage response and growth control: Many tricks in one HAT. *Trends Cell Biol.* **16**, 433–442 (2006).
14. Y. Y. Lin *et al.*, Protein acetylation microarray reveals that NuA4 controls key metabolic target regulating gluconeogenesis. *Cell* **136**, 1073–1084 (2009).
15. A. C. M. Cheung, L. M. Diaz-Santin, Share and share alike: The role of Tra1 from the SAGA and NuA4 coactivator complexes. *Transcription* **10**, 37–43 (2019).
16. H. Wang *et al.*, Structure of the transcription coactivator SAGA. *Nature* **577**, 717–720 (2020).
17. G. Papai *et al.*, Structure of SAGA and mechanism of TBP deposition on gene promoters. *Nature* **577**, 711–716 (2020).
18. Y. Cai *et al.*, Identification of new subunits of the multiprotein mammalian TRRAP/TIP60-containing histone acetyltransferase complex. *J. Biol. Chem.* **278**, 42733–42736 (2003).
19. Y. Doyon, W. Selleck, W. S. Lane, S. Tan, J. Cote, Structural and functional conservation of the NuA4 histone acetyltransferase complex from yeast to humans. *Mol. Cell Biol.* **24**, 1884–1896 (2004).
20. D. Rossetto *et al.*, Eaf5/7/3 form a functionally independent NuA4 submodule linked to RNA polymerase II-coupled nucleosome recycling. *EMBO J.* **33**, 1397–1415 (2014).
21. A. Auger *et al.*, Eaf1 is the platform for NuA4 molecular assembly that evolutionarily links chromatin acetylation to ATP-dependent exchange of histone H2A variants. *Mol. Cell Biol.* **28**, 2257–2270 (2008).
22. P. Xu *et al.*, The NuA4 core complex acetylates nucleosomal histone H4 through a double recognition mechanism. *Mol. Cell* **63**, 965–975 (2016).
23. X. Wang, S. Ahmad, Z. Zhang, J. Cote, G. Cai, Architecture of the *Saccharomyces cerevisiae* NuA4/TIP60 complex. *Nat. Commun.* **9**, 1147 (2018).
24. T. Cao *et al.*, Crystal structure of a nuclear actin ternary complex. *Proc. Natl. Acad. Sci. U.S.A.* **113**, 8985–8990 (2016).
25. K. R. Knoll *et al.*, The nuclear actin-containing Arp8 module is a linker DNA sensor driving INO80 chromatin remodeling. *Nat. Struct. Mol. Biol.* **25**, 823–832 (2018).
26. J. Yuan, K. Chen, W. Zhang, Z. Chen, Structure of human chromatin-remodelling PBAF complex bound to a nucleosome. *Nature* **605**, 166–171 (2022).
27. R. Evans *et al.*, Protein complex prediction with AlphaFold-multimer. *bioRxiv [Preprint]* (2010). <https://doi.org/10.1101/2021.10.04.463034> (Accessed 10 March 2022), p. 463034.
28. B. Li *et al.*, Combined action of PHD and chromo domains directs the Rpd3S HDAC to transcribed chromatin. *Science* **316**, 1050–1054 (2007).
29. J. Huang, S. Tan, Piccolo NuA4-catalyzed acetylation of nucleosomal histones: Critical roles of an Esa1 Tudor/chromo barrel loop and an Epl1 enhancer of polycomb A (EPcA) basic region. *Mol. Cell Biol.* **33**, 159–169 (2013).
30. T. H. Xu *et al.*, Structure of nucleosome-bound DNA methyltransferases DNMT3A and DNMT3B. *Nature* **586**, 151–155 (2020).
31. D. N. Mastronarde, Automated electron microscope tomography using robust prediction of specimen movements. *J. Struct. Biol.* **152**, 36–51 (2005).
32. A. Punjani, J. L. Rubinstein, D. J. Fleet, M. A. Brubaker, cryoSPARC: Algorithms for rapid unsupervised cryo-EM structure determination. *Nat. Met.* **14**, 290–296 (2017).
33. P. D. Adams *et al.*, PHENIX: Building new software for automated crystallographic structure determination. *Acta. Crystallogr. D.* **58**, 1948–1954 (2002).
34. E. F. Pettersen *et al.*, UCSF chimera - A visualization system for exploratory research and analysis. *J. Comput. Chem.* **25**, 1605–1612 (2004).
35. P. Emsley, K. Cowtan, Coot: Model-building tools for molecular graphics. *Acta. Crystallogr. D.* **60**, 2126–2132 (2004).
36. L. M. Diaz-Santin, N. Lukyanova, E. Aciyan, A. C. M. Cheung, Cryo-EM structure of the SAGA and NuA4 coactivator subunit Tra1 at 3.7 angstrom resolution. *Elife* **6**, e28384 (2017).